# Suzaku Observation of the Anomalous X-ray Pulsar CXOU J164710.2–455216

Sachindra Naik*[1], Tadayasu Dotani[1,2,3], Nobuyuki Kawai[3], Motohide Kokubun[1], Takayasu Anada[1], Mikio Morii[4], Tatehiro Mihara[5], Teruaki Enoto[6], Madoka Kawaharada[6] Toshio Murakami[7], Yujin E. Nakagawa[8], Hiromitsu Takahashi[9], Yukikatsu Terada[5], Atsumasa Yoshida[8]

[1]*Institute of Space and Astronautical Science, JAXA, 3-1-1 Yoshinodai, Sagamihara, Kanagawa 229-8510, Japan*

*naik@astro.isas.jaxa.jp*

[2]*Space and Astronautical Science, School of Physical Sciences, The Graduate University for Advanced Studies, 3-1-1 Yoshinodai, Sagamihara, Kanagawa 229-8510, Japan*

[3]*Department of Physics, Tokyo Institute of Technology, 2-12-1 Okayama, Meguro-ku, Tokyo 152-8551, Japan*

[4]*Department of Physics, Rikkyo University, 3-34-1, Nishi-Ikebukuro, Toshima-ku, Tokyo 171-8501, Japan*

[5]*Cosmic Radiation Laboratory, Institute of Physical and Chemical Research, Wako, Saitama 351-0198, Japan*

[6]*Department of Physics, University of Tokyo, 7-3-1 Hongo, Bunkyo-ku, Tokyo 113-0033, Japan*

[7]*Department of Physics, Kanazawa University, Kadoma, Kanazawa, Ishikawa 920-1192, Japan*

[8]*Graduate School of Science and Engineering, Aoyama Gakuin University, Sagamihara, Kanagawa 229-8558, Japan*

[9]*Department of Physical Science, Hiroshima University, 1-3-1 Kagamiyama, Higashi-Hiroshima, Hiroshima 739-8526, Japan*

(Received ; accepted )

**Abstract**

Suzaku TOO observation of the anomalous X-ray pulsar CXOU J164710.2-455216 was performed on 2006 September 23–24 for a net exposure of 38.8 ks. During the observation, the XIS was operated in 1/8 window option to achieve a time resolution of 1 second. Pulsations are clearly detected in the XIS light curves with a barycenter corrected pulse period of 10.61063(2) s. The XIS pulse profile is found to be highly non-sinusoidal. It shows 3 peaks of different amplitudes with RMS fractional ampli-

tude of ∼11% in 0.2–6.0 keV energy band. Though the source was observed with the Hard X-ray Detectors (HXD) of Suzaku, the data is highly contaminated by the nearby bright X-ray source GX 340+0 which was in the HXD field of view. The 1–10 keV XIS spectra are well fitted by two different models consisting of a power-law and a blackbody component and two blackbody components respectively. Although both the models are statistically acceptable, difference in the pulse profiles at soft (0.2–6.0 keV) and hard (6–12 keV) X-rays favors the model consisting of two blackbody components. The temperatures of two blackbody components are found to be 0.61±0.01 keV and 1.22±0.06 keV and the value of the absorption column density is $1.73\pm0.03 \times 10^{22}$ atoms cm$^{-2}$. The observed source flux in 1–10 keV energy range is calculated to be $2.6 \times 10^{-11}$ ergs cm$^{-2}$ s$^{-1}$ with significant contribution from the soft blackbody component ($kT = 0.61$ keV). Pulse phase resolved spectroscopy of XIS data shows that the flux of the soft blackbody component consists of three narrow peaks, whereas the flux of the other component shows a single peak over the pulse period of the AXP. The blackbody radii changes between 2.2–2.7 km and 0.28–0.38 km (assuming the source distance to be 5 kpc) over pulse phases for the soft and hard components, respectively. The details of the results obtained from the timing and spectral analysis is presented.

**Key words:** stars: neutron — stars: pulsars: individual (CXOU J164710.2–455216) — X-rays: general — X-rays: individual (CXOU J164710.2–455216)

## 1. Introduction

The Anomalous X-ray pulsars (AXPs) are a small group of X-ray pulsars which show common properties such as (i) known to present within 1° of the Galactic plane, (ii) pulse period in a very narrow range of 5–12 s, unlike the radio pulsars and accreting X-ray pulsars, (iii) large and more or less steady spin-down or braking, in contrast to most accretion powered pulsars which show spin ups and downs, (iv) similar spectra with soft component characterized by a blackbody model with temperature below 1 keV, with additional harder component in some cases, and (v) relatively high X-ray luminosity (∼$10^{34}$–$10^{36}$ erg s$^{-1}$) which cannot be obtained from the loss of rotational energy of a neutron star alone. Some of the AXPs also emit at optical and/or infrared wavelengths (Hulleman et al. 2000; Durant & van Kerkwijk 2006b). The AXPs are considered to be very young ($10^3$–$10^5$ yr), some of which are associated with supernova remnants (SNRs). The AXPs are considered to be the neutron stars with the strongest known magnetic field ($10^{14}$–$10^{15}$ G), though a direct measurement to confirm the presence of such high magnetic field strengths is still needed. The source of energy for the radiative emission

* Present address: Physical Research Laboratory, Navrangpura, Ahmedabad - 380 009, India

in AXPs is described by the magnetar model, in which the decay of an ultra-strong magnetic field powers the high-luminosity bursts and also a substantial fraction of the persistence X-ray emission (Thompson & Duncan 1996). The competing model for the mechanism of powering the X-ray emission in AXPs is that the AXPs are neutron stars surrounded by fossil disks that were acquired during supernova collapse or during a common-envelope interaction (Corbet et al. 1995; van Paradijs et al. 1995; Chatterjee & Hernqyist 2000). The properties of AXPs are summarized by Mereghetti et al. (2002), Kaspi & Gavriil (2004), Woods & Thompson (2004).

Recently discovered AXP CXOU J164710.2-455216 is located in the young, massive Galactic star cluster Westerlund 1 (Muno et al. 2006). Coherent pulsations with a period of 10.61 s were detected from the 2005 May 22 and June 18 *Chandra* observations of the cluster. The best-fit periods obtained from above two observations were 10.6112(4) s and 10.6107(1) s, which put a limit on the period derivative of $\dot{P} < 2 \times 10^{-10}$ s s$^{-1}$. The 0.5–8.0 keV *Chandra* ACIS spectrum of the AXP was equally well described by a blackbody, power-law, or bremsstrahlung continuum model modified by the interstellar absorption (Muno et al. 2006). Analysis with a more complex model of the magnetar atmosphere suggested that the emission likely arises in one or more hot spots covering a small fraction of the surface (Skinner, Perna, and Zhekov, 2006). Search for an infrared counterpart with the Son of ISAAC instrument on the European Southern Observatory (ESO) New Technology Telescope (NTT) yielded negative result within the $0\farcs3$ uncertainty in the location of the AXP (Muno et al. 2006).

Following the detection of an intense ($\sim 10^{39}$ erg s$^{-1}$) and short (20 ms) burst from CXOU J164710.2-455216 with the Burst Alert Telescope (BAT) on Swift on 2006 September 21 (Krimm et al. 2006), the AXP was observed with various X-ray observatories. Chandra Target of Opportunity (TOO) observation of the AXP on 2006 September 27 showed the presence of 10.61069 s pulsations in the ACIS-S event data (Gavriil et al. 2006). Using the Swift, XMM-Newton, and Chandra data, Israel et al. (2007) obtained a phase-coherent solution for the source pulsations after the burst. The solution required an exponential component decaying with a time scale of 1.4 d, which was interpreted to indicate a recovery stage following a glitch with $\Delta P/P \sim -10^{-4}$. They also detected a spin-down of $\dot{P} \sim 9 \times 10^{-13}$ s s$^{-1}$, which implies a magnetic field strength of $10^{14}$ G. Suzaku performed a TOO observation of the AXP CXOU J164710.2-455216 on 2006 September 23–24. The results obtained from the analysis of the Suzaku observation are presented in this paper.

## 2. Observation

Following the outburst detected by the BAT, Suzaku performed a TOO observation of the AXP CXOU J164710.2-455216 on 2006 September 23 from 06:52 UT to 04:56 UT next day. The TOO observation was carried out at "XIS nominal" pointing position for effective exposures of 38.8 ks with the XIS and 27.7 ks with the HXD. The XIS was operated with "1/8 window" option which gives a time resolution of 1 s, covering a field of view of $17\farcm8 \times 2\farcm2$.

Suzaku, the fifth Japanese X-ray astronomy satellite, was launched on 2005 July 10 (Mitsuda et al. 2007). It covers 0.2–600 keV energy range with the two sets of instruments, X-ray CCDs (X-ray Imaging Spectrometer; XIS) covering the soft X-rays in 0.2–12 keV energy range, and the Hard X-ray Detectors (HXD) which covers 10–70 keV with PIN diodes and 30–600 keV with GSO scintillators. There are 4 XIS (one back illuminated and three front illuminated), each with a 1024 × 1024 pixel X-ray-sensitive CCD detectors at the foci of the each of the four X-ray Telescopes (XRT). The HXD is a non-imaging instrument that is designed to detect high-energy X-rays. It has 16 identical units made up of two types of detectors, silicon PIN diodes (<70 keV) and GSO crystal scintillator (>30 keV). For a detailed description of the XIS and HXD detectors, refer to Koyama et al. (2007) and Takahashi et al. (2007), respectively.

## 3. Analysis and Results

We used public data (rev-1.2) for the Suzaku TOO observation of the AXP CXOU J164710.2-455216 in present work. For the XIS data reduction, the accumulated events were discarded when the telemetry was saturated, data rate was low, the satellite was in the South Atlantic Anomaly (SAA), and when the source elevation above the earth's limb was below 5° with night-earth and below 20° with day-earth. We corrected the known shift of XIS time assignment in rev-1.2 data (7 s for the current data).[1] Applying these conditions, the source spectra were accumulated by selecting a circular region of a radius of 4′.3 around the image center; the circle covers 99% of a point source flux. Using the same circular region, X-ray light curves of 1 s time resolution were also extracted from the XIS event data. Because this extraction circle is larger than the optional window, the effective extraction region is the intersection of the window and this circle. The XIS background spectra were accumulated from the same observation by selecting rectangular regions away from the source. The response files and effective area files for XIS detectors were generated by using the "xissimarfgen" and "xisrmfgen" task of FTOOLS (V6.2). For HXD/PIN data reduction, we used the cleaned event data to obtain the source light curve and spectrum. The simulated background events were used to estimate the HXD/PIN background (Kokubun et al. 2007).

It is found that, during the Suzaku TOO observation, GX 340+0, a bright Z-source which is located at about 21 arcmin away from the AXP, contaminated the HXD data. The RXTE/ASM monitoring data of GX 340+0 shows a more or less constant flux around 30 counts $s^{-1}$. Though GX 340+0 was outside the field-of-view of the XIS, it was well within the HXD field-of-view. Considering a steep power-law spectrum at hard X-rays for AXPs, a roughly estimated 10–50 keV flux of CXOU J164710.2–455216 is found to be a few orders of magnitude lower than that of the observed HXD/PIN flux in above energy band. This suggests that the HXD data of the Suzaku observation of the AXP is significantly contaminated from the

[1] http://www.astro.isas.jaxa.jp/suzaku/analysis/xis/timing/

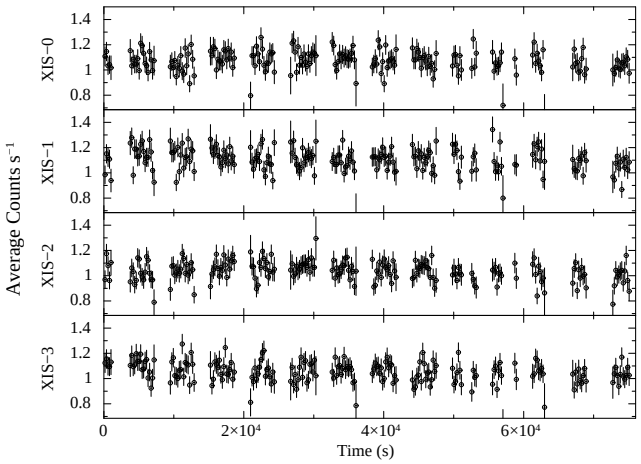


**Fig. 1.** XIS light curves of CXOU J164710.2–455216 obtained from the Suzaku TOO observation of the AXP. The light curves are plotted for a binsize of 200 times the spin period of the AXP.

contribution of the nearby hard X-ray source GX 340+0. In fact, we could not detect significant X-ray pulsation at 10.6106 s in the HXD/PIN data. Therefore, in the present work, we use only the XIS data.

### *3.1. Timing Analysis*

For the timing analysis, a barycentric correction was applied to the arrival times of the X-ray photons using the "aebarycen" task of FTOOLS. As described above, light curves with a time resolution of 1 s were extracted from XIS (0.2–12 keV) event data. Light curves with a binsize of 1, 10, 25, 50, 100, and 200 times the pulse period (10.61063 s) were investigated without any success in finding significant variations of the count rate. The light curve with 200 times the pulse period obtained from all four XIS detectors during the entire observation are shown in Figure 1.

To determine the pulse period of CXOU J164710.2–455216, all four XIS light curves were added together to improve the statistics. As the XISs have very low backgrounds, background subtraction from the light curves was not done. Pulse folding and $\chi^2$ maximization method was first applied to the added XIS light curve using the XRONOS task "efsearch". The result is shown in figure 2. This analysis yielded the pulse period to be 10.61063 s. To improve the estimation of the pulse period, we next applied a phase fitting technique to the XIS data. We divided the XIS light curve into 8 segments and calculated a folded pulse profile for each segment with a common epoch (MJD 54001.000081) and a period (10.61063 s). All the segments have a consistent profile with 3 peaks, but the statistics was poor for the 8th segment, which was not used for the subsequent analysis. We determined the phases of the main peak by fitting a gaussian to the profile. The phases are converted to the relative arrival times of the pulse by multiplying the pulse period. The results are plotted in figure 3 (this is a so-called O–C curve). The slope of the plot indicates the adjustment to the trial period used for the calculation of the

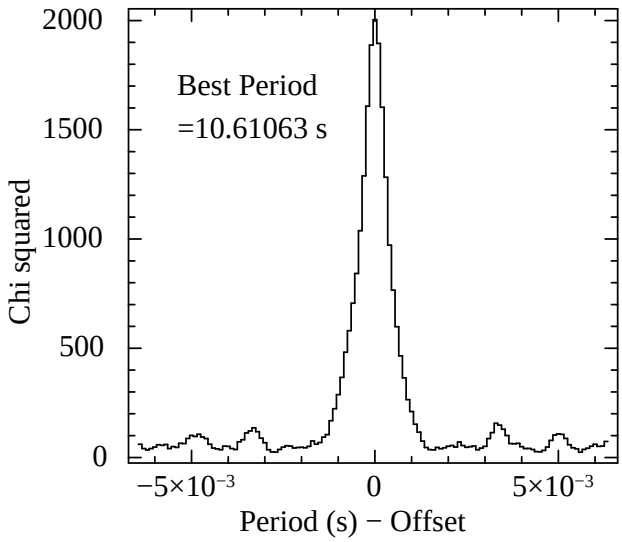


**Fig. 2.** Results of the epoch-folding analysis on the XIS light curve (all four XIS light curves added together) of CXOU J164710.2–455216 obtained from the Suzaku TOO observation of the AXP.

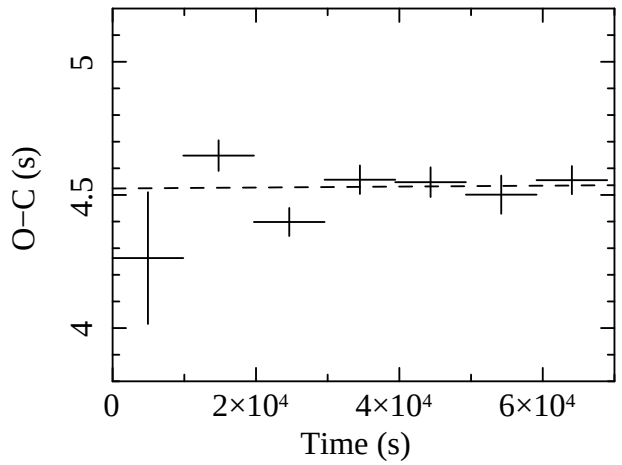


**Fig. 3.** Relative arrival times of the main pulse are plotted when a constant period of 10.61063 s and an epoch of MJD 54001.000081 are assumed. See text for details of the calculation. This plot represents the so-called O–C curve. Broken line is the best-fit linear function to the data, whose slope represents offset of the assumed pulse period from the true one.

**Table 1.** Parameters of the pulse profile

| Component | 0.2–1.8 keV | 1.8–6.0 keV | 6–12 keV |
|---|---|---|---|
| Constant | 0.87 ± 0.03 | 0.86 ± 0.02 | (0.86) |
| Main gaussian | | | |
| Centroid | 0.42 ± 0.01 | 0.43 ± 0.01 | 0.40 ± 0.03 |
| Width | 0.09 ± 0.02 | 0.09 ± 0.01 | 0.16 ± 0.03 |
| Normalization | 0.36 ± 0.05 | 0.41 ± 0.02 | 0.30 ± 0.05 |
| 2nd gaussian | | | |
| Centroid | 0.76 ± 0.02 | 0.74 ± 0.01 | (0.74) |
| Width | 0.06 ± 0.02 | 0.06 ± 0.01 | (0.06) |
| Normalization | 0.15 ± 0.05 | 0.20 ± 0.02 | <0.13 |
| 3rd gaussian | | | |
| Centroid | 1.02 ± 0.02 | 1.03 ± 0.01 | (1.03) |
| Width | 0.08 ± 0.03 | 0.07 ± 0.02 | (0.07) |
| Normalization | 0.14 ± 0.05 | 0.09 ± 0.02 | <0.12 |

Note: Gaussian is defined as $N * \exp\{-(x-c)^2/2w^2\}$, where $N$ is a normalization, $c$ is a centroid, and $w$ is a width. Errors are in 90% confidence limit. Values in the parenthesis are fixed in the fitting.

folded profile. The slope was found to be $0.2 \pm 1.3 \times 10^{-6}$. This means that the pulse period of the AXP was 10.61063(2) s, where the error corresponds to 90% confidence limit. This pulse period is consistent with that obtained from XMM-Newton observation on 2006 September 22 (Muno et al. 2007).

The pulse profile obtained from the added XIS light curve of the Suzaku observation of the AXP is shown in figure 4. The RMS fractional amplitude of the pulse was found to be ∼11%. From the figure, it is observed that the shape of the pulse profile in the XIS energy band (0.2 – 12 keV) is not sinusoidal in nature, rather it has a three peaked profile. Such a three-peaked profile was also observed by XMM-Newton on September 22 (Muno et al. 2007), and Chandra on September 27 (Gavriil et al. 2006). Possibly this is the only AXP which shows a three peaked pulse profile. To investigate the energy dependence of the pulse profile of the AXP, we generated light curves in different energy bands from all four XIS event data. The light curves are folded with the pulse period using the XRONOS task "efold" and the corresponding pulse profiles are shown in Figure 5. The RMS fractional amplitude tends to decrease slightly toward the higher energies: ∼11% in 1.8–6.0 keV while ∼8% in 6–12 keV. The energy resolved pulse profiles in XIS energy band are found to be different, three peaked profiles with different amplitudes in 0.2–6.0 keV energy band and a single peaked profile in 6–12 keV energy band.

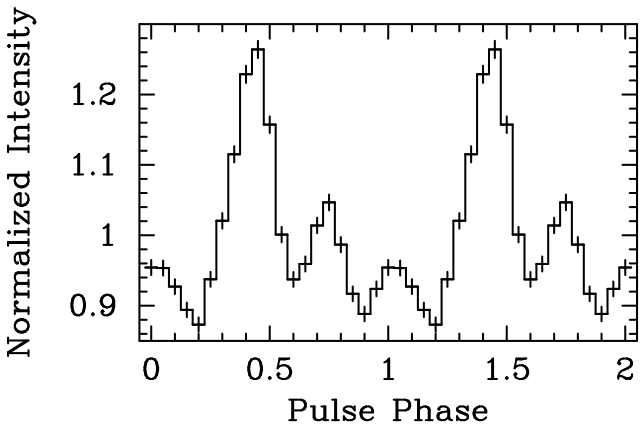


**Fig. 4.** The pulse profile of CXOU J164710.2–455216 obtained from the Suzaku TOO observation of the AXP. The error bars represent $1\sigma$ uncertainties. Two pulses are shown for clarity.

We carried out a model fitting to the pulse profiles to study the energy dependence of the profile quantitatively. We adopted a model consisting of a constant and three gaussian functions to represent the pulse profile. Results of the model fitting was summarized in table 1. We can see in the table that all the model parameters are same within the errors between 0.2–1.8 keV and 1.8–6.0 keV. On the other hand, the profile in 6–12 keV seems to be intrinsically different from those in the lower energy bands. The main peak is significantly broader in 6–12 keV. The 2nd peak, even if present in 6–12 keV, should be significantly smaller than that below 6 keV. Because of these two differences, the pulse profile in 6–12 keV looks more or less sinusoidal. We consider from these differences that the pulse profile in 6–12 keV is intrinsically different from that below 6 keV.

### *3.2. Spectral Analysis*

#### *3.2.1. Pulse phase averaged spectroscopy*

Source and background spectra were extracted from the XIS event files as described in the beginning of the section. The response files and effective area files for XIS detectors were generated by using the "xissimarfgen" and "xisrmfgen" task. Events were selected in the energy ranges of 0.8–10.0 keV for the back illuminated and front illuminated CCDs. After appropriate background subtraction, simultaneous spectral fitting was done for the XIS BI and FI spectra with XSPEC V11. All the spectral parameters other than the relative instrument normalizations, were tied for the BI and FI detectors. Because an artificial structure is known to exist in the XIS spectra around the Si edge, we ignored energy bins between 1.75–1.85 keV in the spectral analysis. The energy bins below 0.8 keV were also ignored because of the lack of photons at soft X-rays.

We tried to fit the XIS spectra of CXOU J164710.2–455216 using a power-law continuum component along with the interstellar absorption. Simultaneous spectral fitting of 0.8–10 keV spectrum with above model yielded a poor fit with reduced $\chi^2$ of 3.9 for 386 degrees of freedom

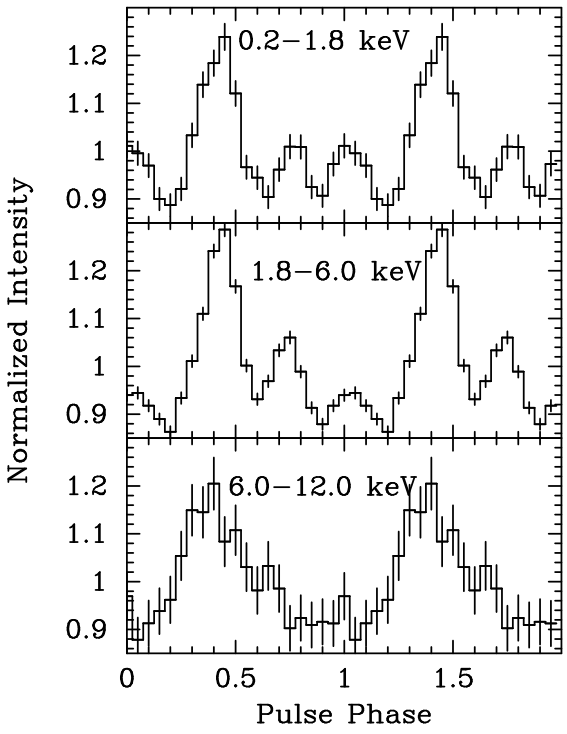


**Fig. 5.** The XIS pulse profiles of CXOU J164710.2–455216 at different energy bands showing the presence/absence of the second and third peaks with energy. No background was subtracted from the folded profiles. The error bars represent 1 sigma uncertainties. Two pulses in each panel are shown for clarity.

(dof). We have tried to fit the spectra with a blackbody model modified with the interstellar absorption. This model improves the spectral fitting with a reduced $\chi^2$ of 2.7 for 386 dof. We tried to fit the spectrum using a model consisting of a blackbody and a power-law component with interstellar absorption. This two-component model provided a best-fit to the XIS spectra of the AXP with a reduced $\chi^2$ of 1.15 for 384 dof. The spectral parameters of the best-fit model obtained from the simultaneous spectral fitting are given in table 2. The count rate spectra of the Suzaku observation is shown in figure 6 along with the model components (top panel) and residuals to the best-fit continuum model (bottom panel). Though the estimated absorption column density is found to be high, the other parameters obtained from the Suzaku observation of the AXP are found to agree to that reported from Chandra and XMM-Newton observations (Gavriil et al. 2006; Muno et al. 2007).

Though the two component model (power-law and blackbody components) fits very well to the 0.8–10.0 keV XIS spectra, this model is not compatible with the energy dependence of the pulse profile. From figure 5, the pulse profile is three peaked at soft X-rays, but tends to be single peaked at hard X-rays. On the other hand, it is found that the power-law component dominates below 2 keV and above 5 keV and the blackbody component dominates in 2–5 keV energy band (Figure 6). This means that the pulse profile should be similar below 2 keV and above 5 keV, which is not the case. Therefore, the model with a blackbody and a power-law

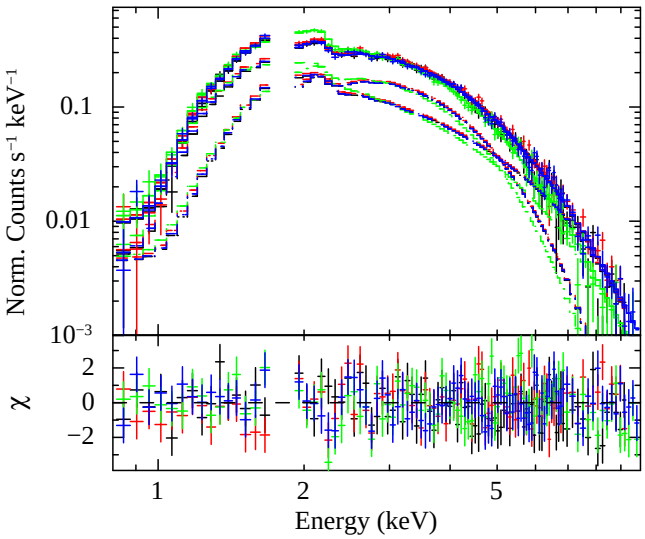


**Fig. 6.** Energy spectrum of CXOU J164710.2–455216 obtained with the four XIS detectors of the Suzaku observation, along with the best-fit model comprising a blackbody component and a power-law continuum model. The bottom panel shows the contributions of the residuals to the $\chi^2$ for each energy bin.

as model components is not favored. Following this, we tried to fit the 1–10 keV spectra with a model consisting of two blackbody components. This model fits the data very well with a reduced $\chi^2$ of 1.19 for 384 dof. The best-fit parameters are given in table 2 and the spectra with the fitted model components are shown in figure 7. The two blackbody model was reported to fit the XMM-Newton data (Muno et al. 2007) and the Swift data (Israel et al. 2007) just after the burst. The best-fit parameters obtained with Suzaku are comparable to those obtained by these satellites.

Addition of a narrow Gaussian function at 6.4 keV (for iron $K_\alpha$ fluorescence line) did not yield any change in the value of the reduced $\chi^2$ and the spectral parameters. The corresponding equivalent width is found to be about 6 eV and the flux of the emission line is estimated to be $8.4\times10^{-15}$ ergs cm$^{-2}$ s$^{-1}$ which is about three orders of magnitude lower than the source flux. This suggests the lack of reprocessing matter surrounding the neutron star to produce iron fluorescence emission.

*3.2.2. Pulse phase resolved spectroscopy*

Different type of pulse profiles of CXOU J164710.2–455216 in different energy bands prompted us to make phase resolved spectral analysis of the Suzaku observation of the AXP. To investigate the changes in the spectral parameters at soft X-rays at different pulse phases, the source spectra were accumulated into 10 pulse phase bins by applying phase filtering in the FTOOLS task XSELECT. The XIS background spectra and response matrices used for the phase averaged spectroscopy, were also used for the phase resolved spectroscopy. Simultaneous spectral fitting was done in the 1–10 keV energy band.

The phase resolved spectra were fitted with the same two blackbody component model used to describe the phase averaged spectrum. The value of the absorption column density ($N_H$)

**Table 2.** Spectral parameters for CXOU J164710.2–455216

| Parameter | Blackbody+Power-law | Blackbody+Blackbody |
|---|---|---|
| $N_H$ ($10^{22}$ atoms cm$^{-2}$) | 2.55±0.01 | 1.73±0.03 |
| $kT_{BB1}$ (keV) | 0.67±0.01 | 0.61±0.01 |
| $kT_{BB2}$ (keV) | —— | 1.22±0.06 |
| Power-law index ($\Gamma_1$) | 3.14±0.08 | —— |
| Blackbody flux ($F_{BB1}$)$^a$ | 1.3±0.1 | 1.8±0.1 |
| Power-law flux ($F_{PO}$)$^a$ | 1.3±0.1 | —— |
| Blackbody flux($F_{BB2}$)$^a$ | —— | 0.8±0.1 |
| Total source flux$^a$ | 2.6±0.1 | 2.6±0.1 |
| Reduced $\chi^2$ | 1.15 (384 dof) | 1.19 (384 dof) |

Note: Errors are defined in $1\sigma$ confidence limit.

$^a$ : Flux (in $10^{-11}$ ergs cm$^{-2}$ s$^{-1}$) is estimated in 1–10 keV energy range without the correction of the absorption.

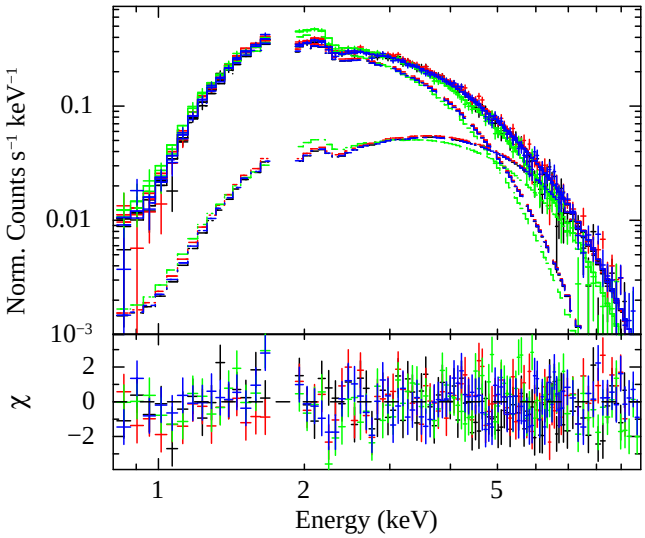


**Fig. 7.** Energy spectrum of CXOU J164710.2–455216 obtained with the four XISs in the Suzaku observation, along with the best-fit model comprising two blackbody components as continuum model. The bottom panel shows the contributions of the residuals to the $\chi^2$ for each energy bin.

and the temperature of the second blackbody component ($kT_2$) did not show any significant variability over the pulse phase. We kept fixed the values of $N_H$ and $kT_2$ to that of the phase average values during the spectral fitting of the phase resolved spectra. The parameters obtained from the spectral fitting to the XIS phase resolved spectra are shown in figure 8 along with the XIS pulse profiles at the top panels, and are listed in table 3. As the soft blackbody component dominates the spectrum at soft X-rays and the second blackbody dominates the spectrum at >5 keV, the change in the estimated flux of the two blackbody components over the pulse period is expected to resemble the pulse profiles at corresponding energy bands. From the figure, it is found that the soft blackbody (marked as BB1 in figure) flux profile shows two prominent and narrow peaks and a third small peak at same phases as in the 0.2–12 keV pulse profile of the AXP. On the otherhand, the second blackbody (BB2) flux shows a single peak profile which is in phase with the 6–12 keV pulse profile of the pulsar. The flux of the soft blackbody takes a maximum in phase 0.4–0.5, whereas that of the second blackbody takes a maximum in phase 0.3–0.4. The blackbody temperature ($kT_{BB1}$) rises from minimum ($\sim$0.59 keV) at phase 0.2–0.3 to maximum ($\sim$0.65 keV) at 0.7–0.8 phase. The radius of the soft blackbody component varies between 2.2 km and 2.7 km and peaks in phase 0.3–0.4. However, the blackbody radius of the second component varies between 0.28 km and 0.38 km, again peaking in phase 0.3–0.4. The radius of the blackbody emitting region is estimated assuming the source distance as 5 kpc. To check the acceptable ranges of the blackbody temperature ($kT_{BB1}$) and the radius of the blackbody emitting region, confidence contours were plotted between $kT_{BB1}$ and blackbody normalization for 0.3–0.4 and 0.7–0.8 phase ranges (figure 9). For the phase 0.3–0.4, the acceptable range of $kT_{BB1}$ and the blackbody normalization ($N_{BB1}$) are found to be 0.57–0.62 keV and 24–33, respectively. However, for phase 0.3–0.4, the acceptable ranges of $kT_{BB1}$ and $N_{BB1}$ are found to be 0.62–0.67 keV and 18.5–24.0, respectively, for 99% confidence limit. The confidence contours for above phase ranges show that the change in the soft blackbody temperature and the radius of the soft blackbody emitting region over pulse phase of the AXP is genuine.

## 4. Discussion

The observed changes in the AXP CXOU J164710.2–455216 before and after the intense and short burst in 2006 September is remarkable. The XMM-Newton observation on 2006 September 22 and the Suzaku observation on 2006 September 23 summaries various changes in the AXP, when compared with the pre-burst data of XMM-Newton on September 16 (Muno et al. 2007). The pulse profile of the AXP was a single peaked before the burst, which changed to a three peaked profile on September 22. These peaks were seen in 0.5–7.0 keV range. Although only the pulse profile below 7 keV was presented in Muno et al. (2007), current Suzaku data show that the pulse profile is single peaked at higher energy band, in 6–12 keV. Because the spectral parameters are comparable between the XMM-Newton data and the Suzaku data, we

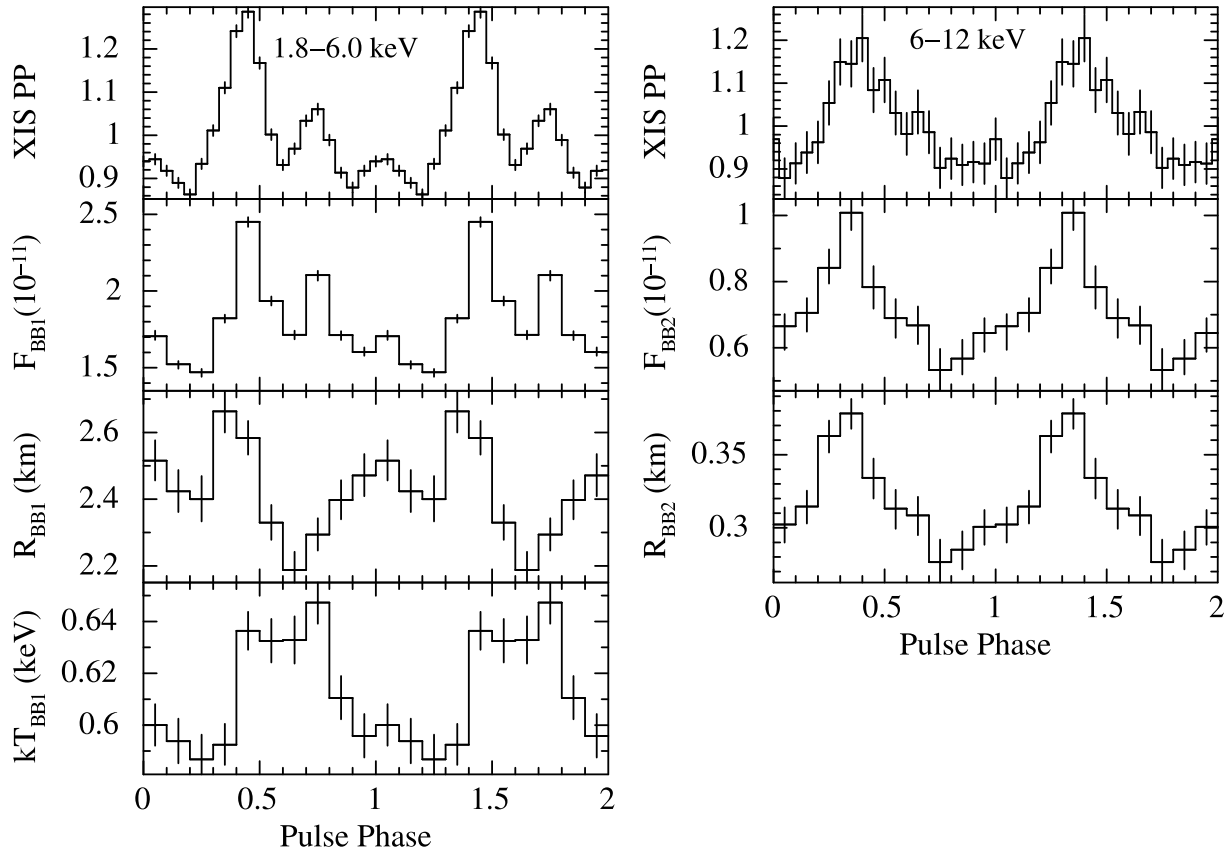


**Fig. 8.** Spectral parameters obtained from the pulse phase resolved spectroscopy of Suzaku observation of CXOU J164710.2–455216. In the figure, the change in the soft blackbody flux ($\mathrm{Flux}_{BB1}$), and second blackbody flux ($\mathrm{Flux}_{BB2}$) over pulse phases are shown along with the blackbody temperature $\mathrm{kT}_{BB1}$ and the radii (assuming the source distance to be 5 kpc) of the blackbody emitting regions ($\mathrm{R}_{BB1}$ and $\mathrm{R}_{BB2}$) with $1\sigma$ errors. The blackbody flux is in the units of $10^{-11}$ ergs cm$^{-2}$ s$^{-1}$. The XIS pulse profiles (XIS PP) in 1.8–6.0 keV and 6–12 keV energy bands are also shown in the left and right top panels respectively.

consider that the nature of the pulse profile, especially the energy dependence, is basically same between these two sets of observations. Though the pulse profiles of some of the AXPs show changes before and after the burst (Kaspi et al. 2003), the change from a single peak profile to a three peak profile is unique to CXOU J164710.2–455216.

Before the intense and short burst, the spectrum was described by a single blackbody component and the pulse profile was single peaked (Muno et al. 2007). The hardening of the source spectrum (after the burst) was seen from the XMM-Newton observations which was explained by adding a power-law component with an index of ∼2.0 to the blackbody component to describe the spectrum. The pulse profile also changed to a three peaked profile as seen from XMM-Newton and Suzaku observations. However, energy resolved pulse profiles of Suzaku observation shows that the hard X-ray (6–12 keV) pulse profile is similar to that of

**Table 3.** Spectral parameters in each pulse phase

| Phase | $F^{*}_{BB1}$ | $F^{*}_{BB2}$ | $R^{\dagger}_{BB1}$ | $R^{\dagger}_{BB2}$ | $kT^{\ddagger}_{BB1}$ |
|---|---|---|---|---|---|
| 0.0 – 0.1 | $1.71^{+0.04}_{-0.02}$ | $0.67^{+0.04}_{-0.07}$ | $2.52 \pm 0.06$ | $0.30 \pm 0.01$ | $0.60 \pm 0.01$ |
| 0.1 – 0.2 | $1.52 \pm 0.03$ | $0.71^{+0.04}_{-0.06}$ | $2.42 \pm 0.06$ | $0.31 \pm 0.01$ | $0.59 \pm 0.01$ |
| 0.2 – 0.3 | $1.47 \pm 0.03$ | $0.84 \pm 0.06$ | $2.40 \pm 0.07$ | $0.36 \pm 0.01$ | $0.59 \pm 0.01$ |
| 0.3 – 0.4 | $1.82 \pm 0.03$ | $1.01 \pm 0.06$ | $2.66 \pm 0.06$ | $0.38 \pm 0.01$ | $0.59 \pm 0.01$ |
| 0.4 – 0.5 | $2.45 \pm 0.03$ | $0.78 \pm 0.07$ | $2.58 \pm 0.05$ | $0.33 \pm 0.01$ | $0.64 \pm 0.01$ |
| 0.5 – 0.6 | $1.94 \pm 0.03$ | $0.69 \pm 0.06$ | $2.33 \pm 0.05$ | $0.31 \pm 0.01$ | $0.63 \pm 0.01$ |
| 0.6 – 0.7 | $1.71 \pm 0.03$ | $0.67 \pm 0.06$ | $2.19 \pm 0.05$ | $0.31 \pm 0.01$ | $0.63 \pm 0.01$ |
| 0.7 – 0.8 | $2.10 \pm 0.04$ | $0.53 \pm 0.06$ | $2.29 \pm 0.05$ | $0.28 \pm 0.02$ | $0.65 \pm 0.01$ |
| 0.8 – 0.9 | $1.71 \pm 0.03$ | $0.57 \pm 0.06$ | $2.40 \pm 0.06$ | $0.29 \pm 0.01$ | $0.61 \pm 0.01$ |
| 0.9 – 1.0 | $1.60 \pm 0.03$ | $0.64 \pm 0.06$ | $2.47 \pm 0.06$ | $0.30 \pm 0.01$ | $0.60 \pm 0.01$ |

Note: Errors are defined in $1\sigma$ confidence limit.

*Flux (in $10^{-11}$ ergs cm$^{-2}$ s$^{-1}$) is estimated in 1–10 keV energy range and is not corrected for absorption.

†In unit of km for the assumed source distance of 5 kpc.

‡In unit of keV.

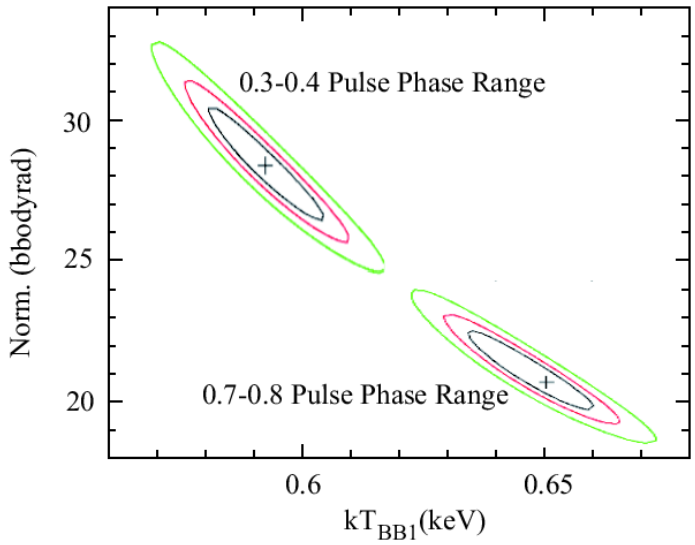


**Fig. 9.** Confidence contours between the normalization and the temperature of the soft blackbody component ($kT_{BB1}$) obtained for the energy spectra in 0.3–0.4 and 0.7–0.8 pulse phase ranges. Normalization is defined as $R^2_{BB1}/D^2_{10}$, where $D_{10}$ is the source distance in unit of 10 kpc. Three contours correspond to 68%, 90%, and 99% confidence limits respectively.

the pre-burst profile obtained from XMM-Newton whereas the soft X-ray pulse profile is found to be three peaked. This energy dependent pulse profile of Suzaku observation ruled out the model with blackbody and power-law as spectral components and favored a model with two blackbody components. The phase resolved spectroscopy of Suzaku observation also showed that the change in the soft blackbody flux over pulse phase shows two narrow and intense peaks and a third minor peak exactly at the same phases of the peaks in the pulse profile. The second blackbody flux, however, shows only a single peak which is similar to the 6–12 keV pulse profile. These findings suggest that the single blackbody component which described both the spectrum and the pulse profile before the outburst is also required to describe the source properties after the outburst with an increased temperature and hence at hard X-ray band. The three peaked profile, seen after the outburst, is interpreted due to the emergence of a new spectral component which dominates at soft X-rays. This new spectral component may be originated from the giant flares in the AXPs/SGRs during which a significant amount of the magnetic energy is released.

The multi-peaked pulse profiles in AXPs/SGRs are attributed to the presence of multi-pole structures of the external magnetic fields. The rearrangement of these multi-pole magnetic fields changes the shape of the observed pulse profiles in these objects. Muno et al. (2007) suggested that the observed changes in pulse profiles and spectral properties of the AXP before and after the burst are due to a change in the distribution of currents in the magnetosphere. This change in magnetosphere is triggered by a plastic motions in the crust of the neutron star. The observed three-peaked profile in the AXP CXOU J164710.2–455216 suggests that three magnetic field foot points developed in response to the change in magnetoshepre. Above the foot points, there might be hot plasma columns, like an accretion column of the accretion powered pulsars. The temperatures distribution is hotter temperature at the lower altitude and lower temperature at the higher altitude. The electron-positron plasma within the column cannot move in the direction perpendicular to the magnetic filed. But those can move in the direction parallel to the magnetic field. Therefore, the X-ray photons pass through along with the magnetic field can escape freely. However, the X-ray photon passing in transversal direction to the magnetic field are restricted by the electron positron scattering. In that case, black body radiation from such foot point is beamed into the magnetic filed direction. This can explain the narrow three-peaked profile of the blackbody flux in CXOU J164710.2–455216.

## Acknowledgments

The authors would like to thank all the members of the Suzaku Science Working Group for their contributions in the instrument preparation, spacecraft operation, software development, and in-orbit instrumental calibration. SN acknowledges the support by JSPS (Japan Society for the Promotion of Science) post doctoral fellowship for foreign researchers (P05249). This work was partially supported by grant-in-aid for JSPS fellows (1705249).

## References


Chatterjee, P. & Hernquist, L. 2000, ApJ, 543, 368

Corbet, R. H. D., Smale, A. P., Ozaki, M., Koyama, K., & Iwasawa, K. 1995, ApJ, 443, 786

Durant, M., & van Kerkwijk, M. H. 2006, ApJ, 652, 576

Gavriil, F. P., Woods, P. M., & Kaspi, V. M. 2006, ATel, 901

Hulleman, F., van Kerkwijk, M. H., & Kulkarni, S. R. 2000, Nature, 408, 689

Israel, G. L., Campana, S., Dall'Osso, S., Muno, M. P., Cummings, J., Perna, R., & Stella, L. 2007, ApJ, 664, 448

Kaspi, V. M., Gavriil, F. P., Woods, P. M., Jensen, J. B., Roberts, M. S. E., & Chakrabarty, D. 2003, ApJ, 588, L93

Kaspi, V. M., & Gavriil, F. P. 2004, Nucl. Phys. B (Proc. Suppl.), 132, 456

Kokubun, M., et al. 2007, PASJ, 59, S53

Koyama, K., et al. 2007, PASJ, 59, S23

Krimm, H., Barthelmy, S., Campana, S., et al. 2006, GCN, 5581

Mereghetti, S., Chiarlone, L., Israel, G. L., & Stella, L. 2002, in Neutron Stars, Pulsars, and Supernova Remnants, ed. W. Becker, H. Lesch, & J. Trumper, 29

Mitsuda, K., et al. 2007, PASJ, 59, S1

Muno, M. P., et al. 2006, ApJ, 636, L41

Muno, M. P., Gaensler, B. M., Clark, J. S., de Grijs, R., Pooley, D., Stevens, I. R., Portegies Zwart, S. F. 2007, MNRAS, 378, L44

Skinner, S. L., Perna, R. & Zhekov, S. A. 2006, ApJ, 653, 587

Takahashi, T., et al. 2007, PASJ, 59, S35

Thompson, C., & Duncan, R. 1996, ApJ, 473, 322

van Paradijs, J., Taam, R. E., & van den Heuvel, E. P. J. 1995, A&A, 299, L41

Woods, P. M., & Thompson, C. 2004, in Compact Stellar X-ray Sources, eds. W. H. G. Lewin & M. van der Klis